metals

MDPI

Article

The Pseudo-Eutectic Microstructure and Enhanced Properties in Laser-Cladded Hypereutectic Ti–20%Si Coatings

Hui Zhang [1,2,*], Zhonghong Zhang [1] and T. M. Yue [2]

1 School of Materials Science and Engineering, Anhui University of Technology, Ma'anshan 243002, China; zrzhhzrzhh@tom.com

2 The Advanced Manufacturing Technology Research Centre, Department of Industrial and Systems Engineering, Hong Kong Polytechnic University, Hung Hom, Hong Kong, China; tm.yue@polyu.edu.hk

* Correspondence: huizhang@ahut.du.cn; Tel.: +86-555-231-1871

Academic Editor: Hugo F. Lopez
Received: 30 November 2016; Accepted: 20 January 2017; Published: 26 January 2017

Abstract: Ti_5Si_3 is an attractive light weight reinforcement phase in hypereutectic Ti–Si-based alloys, however, the proeutectic Ti_5Si_3 phase is brittle and is easily coarsened when the alloy is prepared under normal solidification conditions, thereby limiting its engineering applications in the aviation and biological industries. In this study, a hypereutectic Ti–20%Si coating with a pseudo-eutectic α-Ti + Ti_5Si_3 microstructure was successfully fabricated on a commercially available Ti alloy by laser cladding under non-equilibrium rapid solidification conditions. The fine, rod-like and well-dispersed eutectic Ti_5Si_3 phase, without the primary Ti_5Si_3 phase, that was produced resulted in a considerable improvement in hardness, corrosion resistance, and fracture resistance when compared to the same compositional alloy prepared by the conventional arc melting technique.

Keywords: laser cladding; hypereutectic Ti–Si alloy; corrosion; fracture resistance

1. Introduction

Ti–Si alloys are currently attracting wide academic interest due to their attractive characteristics, such as lightweight, high specific modulus, hardness, corrosion resistance, and good biocompatibility [1–3]. The Ti_5Si_3 intermetallic compound phase, which has a complex D88 hexagonal structure (Mn_5Si_3-type, a1/40.7444 nm, c1/40.5143 nm), has the highest melting temperature (2130 °C), highest hardness (11.3 GPa), and relatively high Young's modulus (225 GPa) among the five silicide phases, $TiSi_2$, TiSi, Ti_5Si_4, Ti_5Si_3, and Ti_3Si, that exist in the binary Ti–Si alloy system [4]. Thus, it could act as a desired reinforcement phase to significantly increase the hardness of the ductile titanium matrix. Evidently, the higher the Ti_5Si_3 phase content, the higher the hardness of the Ti–Si alloy. Indeed, hypereutectic Ti–Si alloys dominated by Ti_5Si_3 have received much attention in recent years, including applications as coating materials [2–5]. Nevertheless, the proeutectic Ti_5Si_3 phase nucleated from the liquid metal may develop into coarse particles, and result in low toughness of the alloy, which could restrict its applications [2,4]. It is believed that, if one can refine the Ti_5Si_3 phase in hypereutectic alloys and avoid the formation of coarse primary Ti_5Si_3 crystals, then the toughness of the alloy can be improved.

Based on the Ti–Si phase diagram [4,6], the eutectic reaction of the alloy occurs approximately at 13.5 atom % Si (atomic). This study aims to achieve the refinement of the Ti_5Si_3 eutectic phase as well as to suppress the nucleation of the primary Ti_5Si_3 phase of a Ti–20 atom % Si hypereutectic alloy using laser cladding. It is envisaged that, due to the nature of laser processing, i.e., under rapid solidification conditions, this aim can be achieved. This study also compares the hardness, fracture

toughness, and corrosion resistance of the coating to those of the same compositional alloy prepared by the conventional arc melting and metal mold casting method.

2. Materials and Methods

The Ti–20 atom % Si alloy was prepared by both laser cladding and arc melting methods. For laser cladding, a continuous-wave CO_2 laser system was used to prepare the coating on a commercially available titanium Ti alloy (TC21) substrate. The Ti substrate was a square block (100×100 mm^2) with a thickness of 10 mm, of the nominal composition Ti–6Al–2Sn–2Zr–3Mo–1Cr–2Nb–0.1Si. It is an $\alpha + \beta$ titanium alloy with high strength and toughness, as well as high fatigue tolerance [7]. The Ti and Si powders used in the laser cladding had a purity of 99.7 wt % with particle sizes ranging between 50 and 120 μm. They were mechanically mixed, dried in a vacuum oven for 12 h, and delivered to the laser processing zone using a lateral powder feeder. High-purity argon gas flowing through a coaxial nozzle created a shielding region on the substrate to prevent oxidation of the powder. The laser cladding parameters used were as follows: a laser power of 2 kW, a laser beam diameter of 4 mm, a laser scan speed of 400 mm·min^{-1}, a laser track overlap ratio of 40%, and a powder feed rate of 200 mg/s. A single-layer coating was produced using one deposition pass by overlapping the laser tracks, resulting in a coating thickness of about 1.1 mm. Meanwhile, for the preparation of the cast material, high purity elements (Fe 99.9% and Si 99.9%) were used to obtain 25 g castings. The Ti–20 atom % Si alloy was prepared by means of Ti-gettered arc melting, where the molten alloy, produced using a non-consumable vacuum arc melting furnace (Shenyang Vacuum Technology Institute, Shenyang, China), was drop-cast into a 20 mm diameter copper mold. The melting was repeated four times to improve the chemical homogeneity of the alloy.

The phases and microstructure were characterized using a X-ray diffractometer (Rigaku, Tokyo, Japan) with Cu Kα radiation operated at 40 kV and 30 mA, and a JSM-6490 scanning electron microscope (JEOL, Tokyo, Japan) equipped with an energy dispersive spectrometer (EDAX, Mahwah, NJ, USA). The Vickers indentation technique was used, with an applied load of 4.9 N, to measure the hardness of the specimens, which were annealed for 2 h at 300 °C to relieve the residual stresses prior to the test. The indentation cracking-based method was used to evaluating the crack extension resistance (toughness) of the cast and laser-cladded specimens [8]. The test was performed using a loading force of 294 N to provoke crack nucleation. The electrochemical polarization measurements were carried out using a three-electrode cell system in Tyrode's artificially simulated body fluid solution at room temperature.

3. Results and Discussion

3.1. Characterization of Microstructure and Phases

An examination of the microstructure of the metal mold cast material showed that it consists of large grains with a coarse Ti_5Si_3 phase. Figure 1a shows two of such large columnar grains with a width of about 3 mm. An etched specimen revealed that it consists of coarse primary Ti_5Si_3 particles with sharp edges distributed in a α-Ti + Ti_5Si_3 eutectic matrix (Figure 1b). The primary Ti_5Si_3-phase, as marked by arrows, are about 15 μm in width, and more than 100 μm in length was nucleated from the liquid phase as the alloy experienced a eutectic reaction: Liquid → Ti_5Si_3 + β-Ti at 1330 °C [4,6]. The β-Ti subsequently transformed to α-Ti at a lower temperature. Figure 1c shows that the size of the Ti_5Si_3-phase in the eutectic matrix is about 3 μm in width and 10 μm in length.

Turning to the laser-cladded coating. Figure 2a shows the overall morphology of the microstructure of a cross section of a laser-cladded specimen. Here, the Ti–20%Si coating, the laser melted zone (LMZ), the heat affected zone (HAZ), and the unaffected substrate can be identified. The coating is free from porosity and cracks, and a metallurgical bonded interface was formed between the LMZ and the coating. The microstructure of the LMZ changed from equiaxed to columnar crystal growth towards the coating layer. This is thought to be due to the fact that, during the solidification of

the LMZ, the crystal growth velocity increases with increasing distance from the bottom of the LMZ. A very narrow HAZ (about 400 μm) was observed between the substrate and the LMZ; this agreed with the hardness measurements obtained across the section of a coated specimen, and the results are presented in the next section. It was also observed that a continuous interface was formed between the overlapped regions between two laser tracks, and no cracks were found (Figure 2b).

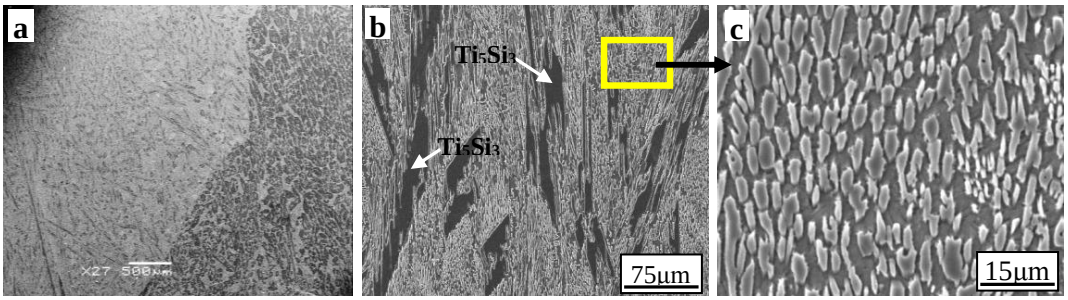

Figure 1. Microstructure of the Ti–20%Si alloy cast in metal mold showing (**a**) large grains; (**b**) a coarse primary Ti_5Si_3 phase; and (**c**) the eutectic matrix.

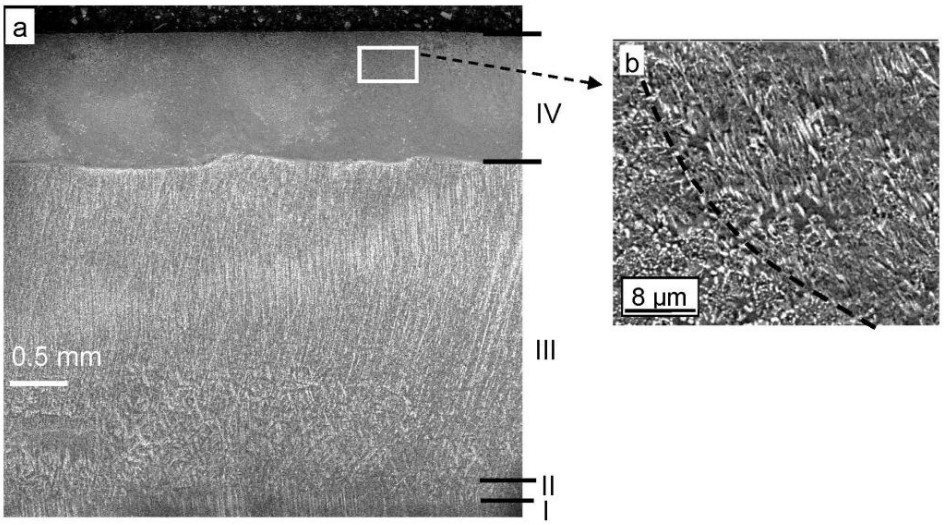

Figure 2. Cross-sectional images of the laser-cladded specimen showing (**a**) the unaffected substrate (I), the heat affected zone (II), the laser melted zone (III), the Ti–20% Si coating (IV); and (**b**) a laser overlapped region.

A closer examination of the coating microstructure shows that it exhibits a fine pseudo-eutectic microstructure. When compared to that of the metal mold casting, the laser-cladded material has a well-dispersed eutectic Ti_5Si_3 phase, which was greatly refined to the submicron level and has a rod-like growth morphology, suggesting that the formation of the primary Ti_5Si_3 phase was suppressed (Figure 3a,b). The eutectic phase has a kind of cellular structure having a size of about 10 μm. The formation of a eutectic structure, without the coarse primary Ti_5Si_3 phase, is considered to be due to non-equilibrium solidification conditions. During laser cladding, the outgrowth speed of the solid–liquid (S/L) interface is high and the local solidification time is limited, with large undercooling in front of the S/L interface. Thus, the sluggish diffused solute atoms accumulated at the liquid zone ahead of the S/L interface cannot be redistributed to the liquid region fast enough, causing the nucleation rate to decrease and suppress the nucleation of the Ti_5Si_3 phase [9]. Moreover, as the Ti–Si alloy belongs to a metal–nonmetal system, the non-faceted interface of the α-Ti grain grew more quickly than that of the faceted interface of the Ti_5Si_3 phase under the condition of large

undercooling [9]. Therefore, crystallization occurs by diffusion decomposition into a mixture of crystals of α-Ti + Ti_5Si_3 phases that preceded the growth of the primary Ti_5Si_3 phase and resulted in the growth of a pseudo-eutectic structure in the Ti–20%Si alloy. The X-ray diffraction (XRD) patterns shown in Figure 4 indicate that both the metal mold cast and laser-cladded materials, primarily composed of α-Ti and Ti_5Si_3 phases without the Ti_3Si phase, suggests that the peritectoid reaction, Ti_5Si_3 + β-Ti → Ti_3Si, was supressed.

It is also worth noting that the rapidly solidified Ti–20%Si laser clad layer is metallurgically bonded to the TC21 alloy substrate (Figure 3c). The microstructure close to the substrate-coating interface has a typical hypoeutectic microstructure with a proeutectic α-Ti phase. The energy dispersive spectrometer (EDS) analysis shows that the Ti content in this area reached 89 atom %, which is higher than the nominal composition of the coating alloy. This is due to the remelting of the substrate and the alloy dilution effect. Such dilution at the interface is desirable, because the proeutectic α-Ti phase is relatively ductile and can decrease the tendency of cracking at the coating-substrate interface that may be caused by the differences in thermophysical properties.

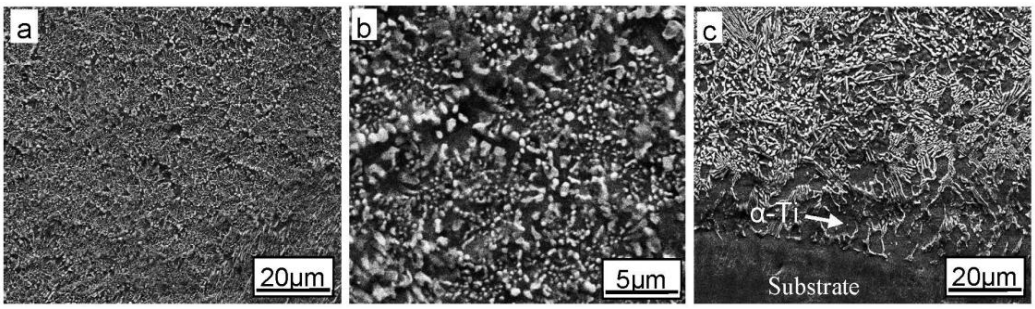

Figure 3. (**a**) Microstructure of the Ti–20%Si laser clad coating; (**b**) a higher magnification of (**a**) showing the fine eutectic structure; (**c**) the interface between the coating and the substrate.

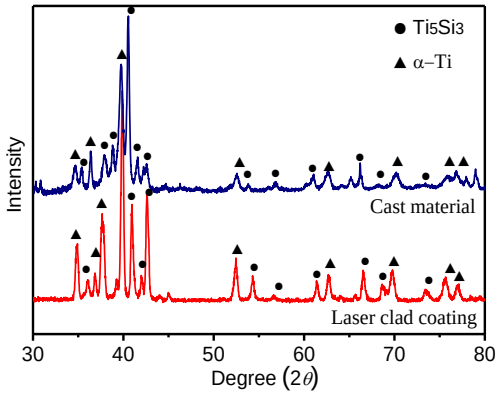

Figure 4. XRD patterns of the Ti–20%Si alloys.

3.2. Hardness and Fracture Resistance

Figure 5 presents the microhardness profile across a laser-cladded specimen, in which the hardness of the coating reached 672 $HV_{0.5}$. This hardness value is double that of the TC21 substrate (322 $HV_{0.5}$) and was approximately 30% higher than that of the metal mold cast material (504 $HV_{0.5}$). The hardness values of the remelted and HAZ zones were 389 $HV_{0.5}$ and 352 $HV_{0.5}$, respectively, which are actually higher than that of the substrate. This could be due to the refinement of the microstructure. Further, the high hardness obtained for the coating was a consequence of the rapid solidification rate in laser cladding (10^3–10^5 °C/s), which is much higher than that normally obtained in the arc melting-metal mold process (10^2 °C/s) [10,11]. Rapid solidification results in a much refined and well-distributed Ti_5Si_3 hard phase in the eutectic microstructure.

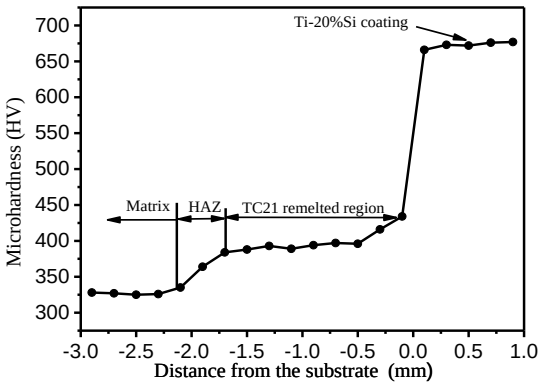

Figure 5. Hardness profile of a laser-cladded specimen.

Figure 6 shows the results of the indentation cracking test for the metal cast and laser-cladded materials. For the former, many microcracks developed at the tip of the indentation in the primary Ti_5Si_3 particles (Figure 6a,b), as well as across the coarse eutectic phase, within and close to the indentation (Figure 6c). It is believed that the stress concentration at the corner of the indentation can readily lead to nucleation of the cracks in the coarse primary Ti_5Si_3-phase. This indicates the brittle nature of coarse Ti_5Si_3 particles; this is consistent with findings of previous studies that the fracture toughness of Ti_5Si_3 particles decreased from 5 to 2.1 MPa·$m^{1/2}$ when the particle size increased from 6 μm to 20–50 μm [12–14].

On the other hand, no macrocracks, as were found in the cast material, were observed at the corner of the indentation of the laser-cladded material (Figure 6d), suggesting that the absence of coarse primary Ti_5Si_3 particles and the refined submicron size of the pseudo-eutectic Ti_5Si_3 phase effectively suppress nucleation of the cracks. This could improve the toughness of the hypereutectic Ti–20%Si alloy. Figure 6e shows a higher magnification image of the marked area in Figure 6d, where a microcrack developed along a diagonal edge of the indentation where a high concentration of stresses is present. However, the crack did not cut through the fine Ti_5Si_3 phase, but propagated along its interface, which resulted in a tortuous crack propagation path. It is believed that this kind of crack growth phenomenon can give rise to a higher toughness for the laser-cladded material.

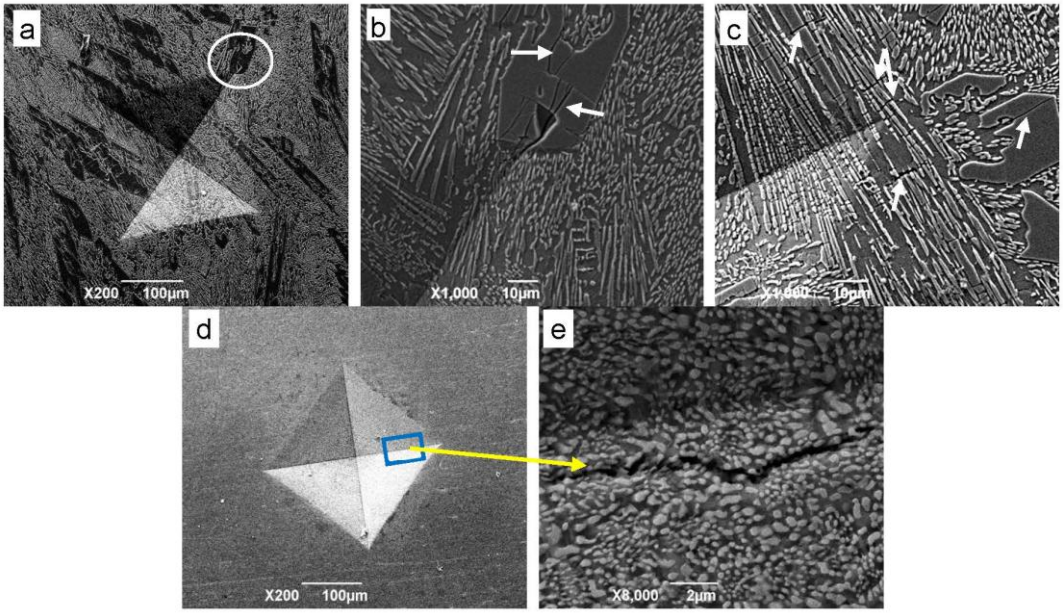

Figure 6. Cracks developed after the indentation test: (**a**,**b**) at the tip of the indentation, and (**c**) inside and around the indentation (cast material); (**d**,**e**) a microcrack developed along an edge (laser clad).

3.3. Corrosion Resistance in the Simulated Body Fluid Solution

Figure 7 presents the potentiodynamic polarization curves of the TC21 substrate and the Ti–20%Si specimen. The free corrosion potential (E_{corr}) and the corrosion current density (I_{corr}) of the coating material were −0.298 V and 0.31 μA·cm^{-2}, respectively, whereas, for the substrate materials, the values were −0.450 V and 0.86 μA·cm^{-2}. These figures show that the corrosion resistance of the former is much higher than that of the latter. The results are consistent with previous research work in which the formation of the Ti–Si compound contributed to the increase of E_{corr}, and a decrease in I_{corr} in Ti alloys corroded in a simulated body fluid [15–17]. In this study, it was also found that the laser-cladded material with a refined pseudo-eutectic microstructure has superior corrosion resistance to the cast material of the same composition. The E_{corr} and I_{corr} of the cast material were −0.327 V and 0.78 μA·cm^{-2}, respectively. When comparing these to those of the laser-cladded material, the corrosion potential of the cladded material was approximately 30 mV more noble than that of the cast material, and its current density was about half that of the cast material.

In addition, the linear polarization results also showed that the coating material exhibited a relatively large passive range when compared to the cast material. For the cast material, the passive range, as indicated by the arrows (from −0.25 to 0.0 V), is 0.25 V, while it is over 0.45 V (from −0.1 to 0.35 V) for the laser-cladded material. The extended passive range indicates that a more stable protective corrosion film formed on the laser clad coating, owing to the fine and well-distributed eutectic Ti_5Si_3 phase.

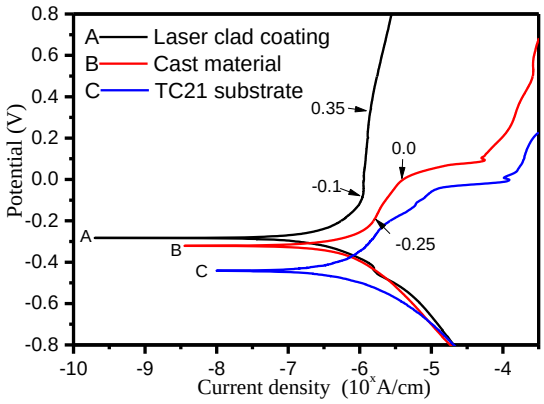

Figure 7. A comparison of the potentiodynamic polarization plots of the TC21 substrate and the Ti–20%Si alloys produced by laser cladding and metal mold casting.

4. Conclusions

(1) A pseudo-eutectic (α-Ti + Ti_5Si_3) microstructure was obtained in the hypereutectic Ti–20%Si coating produced by laser cladding. Unlike the metal cast material, coarse primary Ti_5Si_3 crystals are absent.

(2) The fine and well dispersed eutectic Ti_5Si_3 phase of the laser-cladded material greatly improves the hardness, corrosion resistance, and fracture resistance of the hypereutectic Ti–20%Si when compared with the same alloy prepared by the conventional metal mold casting method.

Acknowledgments: The work described in this paper was substantially supported by the research grant from the Hong Kong Polytechnic University (Project No. G-YM71), the authors also appreciate the support of the Joint Fund of Iron and Steel Research by the National Natural Science Foundation of China under Grant No. U1560105.

Author Contributions: T.M. Yue and Hui Zhang conceived and designed the experiments; Zhonghong Zhang and Hui Zhang performed the experiments; T.M. Yue and Hui Zhang analyzed the data; T.M. Yue and Hui Zhang wrote the paper.

Conflicts of Interest: The authors declare no conflict of interest.

References

1. Wang, X.; Wang, L.; Wang, Q.J.; Wu, Y.D.; Si, J.J.; Hui, X.D. Enhanced mechanical properties and structure stability induced by Si in Ti–8.5Al–1.5Mo alloys. *Mater. Eng. Sci. A* **2016**, *676*, 304–311. [CrossRef]
2. Alhammad, M.; Esmaeili, S.; Toyserkani, E. Surface modification of Ti–6Al–4V alloy using laser-assisted deposition of a Ti–Si compound. *Surf. Coat. Technol.* **2008**, *203*, 1–8. [CrossRef]
3. Hu, Z.H.; Zhan, Y.Z.; She, J. The role of Nd on the microstructural evolution and compressive behavior of Ti–Si alloys. *Mater. Eng. Sci. A* **2013**, *560*, 583–588. [CrossRef]
4. Kishida, K.; Fujiwara, M.; Adachi, H.; Tanaka, K.; Inui, H. Plastic deformation of single crystals of Ti_5Si_3 with the hexagonal D88 structure. *Acta Mater.* **2010**, *58*, 846–857. [CrossRef]
5. Riley, D.P. Synthesis and characterization of SHS bonded Ti_5Si_3 on Ti substrates. *Intermetallics* **2006**, *14*, 770–775. [CrossRef]
6. Murray, J.L. *Phase Diagrams of Binary Titanium Alloys*; ASM International: Materials Park, OH, USA, 1987; p. 289.
7. Zhang, Q.; Chen, J.; Zhao, Z.; Tan, H.; Lin, X.; Huang, W.D. Microstructure and anisotropic tensile behavior of laser additive manufactured TC21 titanium alloy. *Mater. Eng. Sci. A.* **2016**, *673*, 204–212. [CrossRef]
8. Tancret, F.; Osterstock, F. The Vickers indentation technique used to evaluate thermal shock resistance of brittle materials. *Scr. Mater.* **1997**, *37*, 443–447. [CrossRef]
9. Herlach, D.M. Non-equilibrium solidification of undercooled metallic melts. *Mater. Eng. Sci. R* **1994**, *12*, 177–272. [CrossRef]
10. Zhang, H.; He, Y.Z.; Pan, Y. Enhanced hardness and fracture toughness of the laser-solidified $FeCoNiCrCuTiMoAlSiB_{0.5}$ high-entropy alloy by martensite strengthening. *Scr. Mater.* **2013**, *69*, 342–345. [CrossRef]
11. Si, S.H.; Zhang, H.; He, Y.Z.; Li, M.X.; Guo, S. Liquid Phase Separation and the Aging Effect on Mechanical and Electrical Properties of Laser Rapidly Solidified $Cu_{100-x}Cr_x$ Alloys. *Metals* **2015**, *5*, 2119–2127. [CrossRef]
12. Zhang, L.; Wu, J. Ti_5Si_3 and Ti_5Si_3-based alloys: Alloying behavior, microstructure and mechanical property evaluation. *Acta Mater.* **1998**, *46*, 3535–3546. [CrossRef]
13. Frommeyer, G.; Rosenkranz, R.; Smarsly, W. Microstructure and properties of high melting point intermetallic Ti_5Si_3 and $TiSi_2$ compounds. *Mater. Sci. Eng. A* **1992**, *152*, 288–294.
14. Counihan, P.J.; Crawford, A.; Thadhani, N.N. Influence of dynamic densification on nanostructure formation in Ti_5Si_3 intermetallic alloy and its bulk properties. *Mater. Sci. Eng. A* **1999**, *267*, 26–35. [CrossRef]
15. Xu, J.; Liu, L.; Li, Z.; Munroe, P.; Xie, Z.H. Niobium addition enhancing the corrosion resistance of nanocrystalline Ti_5Si_3 coating in H_2SO_4 solution. *Acta Mater.* **2014**, *63*, 245–260. [CrossRef]
16. Xu, J.; Liu, L.L.; Xie, Z.H.; Munroe, P. Nanocomposite bilayer film for resisting wear and corrosion damage of a Ti–6Al–4V alloy. *Surf. Coat. Technol.* **2012**, *206*, 4156–4165. [CrossRef]
17. Wu, Y.; Wang, A.H.; Zhang, Z.; Zheng, R.R.; Xia, H.B.; Wang, Y.N. Laser alloying of Ti–Si compound coating on Ti–6Al–4V alloy for the improvement of bioactivity. *Appl. Surf. Sci.* **2014**, *305*, 16–23. [CrossRef]